JOURNAL OF APPLIED ELECTROCHEMISTRY 11 (1981) 23–32

Behaviour of lead electrodes in sulphate electrolytes. II. Investigation of the electrode kinetics

S. FLETCHER*, D. B. MATTHEWS

School of Physical Sciences, The Flinders University of South Australia, Bedford Park, South Australia 5042, Australia

Received 6 May 1980

The behaviour of lead electrodes in 0.5 M sulphuric acid has been investigated. The electrodes were of the type III variety, which were prepared by alternately cycling the lead electrodes through the $Pb/PbSO_4$ potential and hydrogen evolution. On these electrodes and at this concentration of electrolyte it proved possible to record highly reproducible experimental data. Various techniques were employed to investigate the $Pb \rightarrow PbSO_4$ reaction, including linear potential scans and potential steps. The electrode kinetics are discussed and, where possible, compared with theoretical models.

1. Introduction

In earlier publications [1, 2] we proposed a new model for the nucleation and growth of thick crystalline films in electrochemistry. A key feature of the new model was the assumption that crystals grew in a shape-preserving way. Thus the rates of lateral and vertical spreading were assumed to be 'locked together' via the crystallography of the growing crystal. In the model the rate-determining step was taken to be the spreading of the basal plane of the crystal at the electrode surface. Crystal growth into the third dimension (i.e. away from the electrode surface) was viewed as 'fast', but constrained by the crystallography of the growth shape. These assumptions led to the calculation of a volume transformation, which described the volume of crystals including intercrystal collisions in terms of the normalized basal areas of crystals considered independently. The volume transformation takes the form

$$V_T \propto \rho^{-1/2} [1 - \exp(-\theta_X)]^{3/2} \quad (1)$$

where V_T is the transformed volume of crystals, ρ is the density of crystals in the 2D plane of the electrode surface, and θ_X is the sum of the normalized basal areas of crystals considered independently. (In the derivation of Equation 1, the distribution of crystal centres was assumed to be a homogeneous Poisson point process in 2D.) One advantage of Equation 1, compared with an earlier model [3], was the fact that it was not necessary in invoke some sort of diffusion control to growth sites in the crystal as a necessary feature of the mathematical models.

For the case of the instantaneous appearance of nuclei at $t = 0$, Equation 1 led to a potentiostatic current–time transient of the form

$$i \propto t \exp(-t^2) [1 - \exp(-t^2)]^{1/2} \quad (2)$$

in which the i–t transient maximum parameters i_m and t_m varied as

$$i_m \propto (\alpha/\rho)^{1/2} k \quad (3)$$

$$t_m \propto (1/\alpha)^{1/2} k^{-1} \quad (4)$$

and the total charge passed in creating a complete layer behaved as

$$q_{Total} \propto \rho^{-1/2}. \quad (5)$$

In the above equations α is a constant, ρ is the density of crystals in the 2D plane of the electrode surface, and k is the spreading rate of the crystals in some specified linear direction. Furthermore,

$$\theta_X = \alpha \left(\int_0^t k \, dt \right)^2, \qquad k = \text{constant}. \quad (6)$$

For the case of progressive nucleation, Equation 1 led to a potentiostatic current–time transient which could only be evaluated numerically; the

* Present address: CSIRO Division of Mineral Chemistry, PO Box 124, Port Melbourne, Victoria 3207, Australia.

0021–891X/81/010023–10$03.00/0

i–t curve was given by the first derivative with respect to time of the expression

$$q \propto \left[\int_0^t A \exp(-Ak^2t^3)\mathrm{d}t\right]^{-1/2} \times [1-\exp(-Ak^2t^3)]^{3/2} \quad (7)$$

and an approximate treatment for the i–t transient maximum parameters led to expressions of the type

$$i_m \propto k \quad (8)$$

$$t_m \propto (Ak^2)^{-1/3} \quad (9)$$

$$i_m^2 t_m^3 \propto A^{-1}. \quad (10)$$

It was also found that

$$q_{\text{Total}} \propto (k/A)^{1/3}. \quad (11)$$

In the above expression A is the appearance rate of crystals.

In the present work we compare some predictions of the above model to a physical system of interest, namely the formation of $PbSO_4$ on Pb in sulphate electrolytes. As we shall see, the real situation is much more complex than that suggested by the above model alone, but nevertheless some interesting conclusions can be drawn.

2. Experimental

The experimental conditions were the same as those described in our previous paper [4]. However for quantitative measurements in the present work an additional positive-feedback iR compensation circuit was introduced in order to compensate for the electrolyte component of the iR drop. The lead electrodes employed were principally of the type III variety, whose preparation and discriminant curve cyclic voltammetry DCCV were previously described. The kinetic behaviour of type III electrodes has not been previously described, but note that it is sufficiently different to that described by other workers, who used different lead surfaces, that direct comparison with their data is not attempted. For a comparison of type III electrodes with types I and II, the reader is referred to Part 1 [4].

3. Results

As we showed in our previous paper, lead electrodes vary widely in the magnitude of their i–η–t responses depending on the electrode pretreatment procedure employed [4]. After applying a wide variety of potential perturbations to a series of electrodes, it was found that only electrodes classified as type III could be restored to a reproducible surface condition without removing the electrode from the cell and retreating it. (To restore this electrode to a reproducible condition it was only necessary to evolve hydrogen on it for short periods of time, usually a few minutes.) On the other hand type I and type II electrodes showed erratic behaviour after the application of various different potential–time profiles, with the result that current responses were irreproducible. Furthermore, type I and type II electrodes exhibited alarming sensitivity toward the effects of hydrogen evolution. Thus type III electrodes were a natural choice for the present work. It was found that, given appropriate care, reproducibilities of the order of 2 or 3% could readily be obtained with such electrodes.

3.1. *Cyclic voltammetry*

In Figs. 1a and b we compare steady voltammograms obtained on type I and type III electrodes. The scan rates in both cases were identical, as were the scan limits of −1000 mV and 0 mV versus SCE. In both figures two successive scans are superimposed, which gives an indication of the reproducibility obtained. The most obvious difference between the two electrodes is the absolute magnitude of i_p; the type III electrodes exhibit an i_p approximately 25 times larger than that of type I electrodes. That this difference did not arise (for the most part) as a result of differences in surface area is shown in Fig. 2. The data in this figure were obtained by evolving hydrogen in eight bursts of five minutes each on an initially type I electrode. Between the hydrogen evolution treatments 20 scans were made (on each occasion) under the conditions of Fig. 1, and each time i_p was recorded on the sixth cycle. The type I electrode slowly transformed into a type II electrode and eventually (not shown in the figure) a type III electrode. However, this progression in i_p to higher and higher values was not matched by changes in the hydrogen evolution currrent, which increased only by a factor of about 30% during this process. If the hydrogen evolution reaction had introduced a surface roughening process, and this was entirely respon-

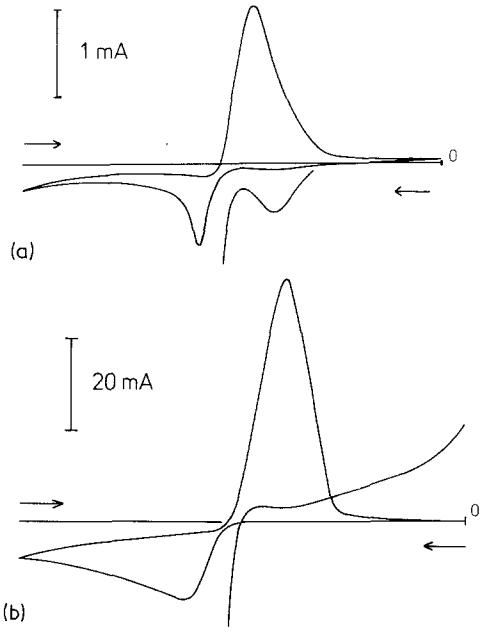

Fig. 1. (a) Reproducible voltammogram recorded on a type I electrode in 0.5 M H_2SO_4. Scans from -1000 mV to 0 mV versus SCE at 200 mV s^{-1}. Inset magnified 10 × for clarity (*iR* drop $\simeq 1.2\ \Omega$). (b) Reproducible voltammogram recorded on a type III electrode in 0.5 M H_2SO_4. Scans from -1000 mV to 0 mV versus SCE at 200 mV s^{-1}. Incomplete scan magnified 40 × for clarity (*iR* drop $\simeq 1.2\ \Omega$).

sible for the increase in i_p, then it would have been expected that the percentage change in hydrogen evolution current (30%) would be identical with the change in the Pb → $PbSO_4$ current (2500%), which was manifestly not the case. Thus the remarkable difference in i_p observed between type I and type III electrodes cannot be simply ascribed to a surface area effect. Since we already know that hydrogen evolution produces localized pitting of lead surfaces [4], we suggest therefore that the pits influence the Pb → $PbSO_4$ transition in some way not immediately connected with simple surface area considerations, e.g. by providing preferential sites at which the overall crystal growth of $PbSO_4$ can proceed in an accelerated way.

Another interesting feature of Figs. 1a and b is the presence of *two* peaks on the backward scan from 0 mV to -1000 mV versus SCE. The smaller peak is shown amplified 10× in Fig. 1a and is shown amplified 40× in Fig. 1b. Whatever process this peak might correspond to, it is unaffected by the hydrogen evolution pretreatment since its height is comparable in both figures, about 50 μA.

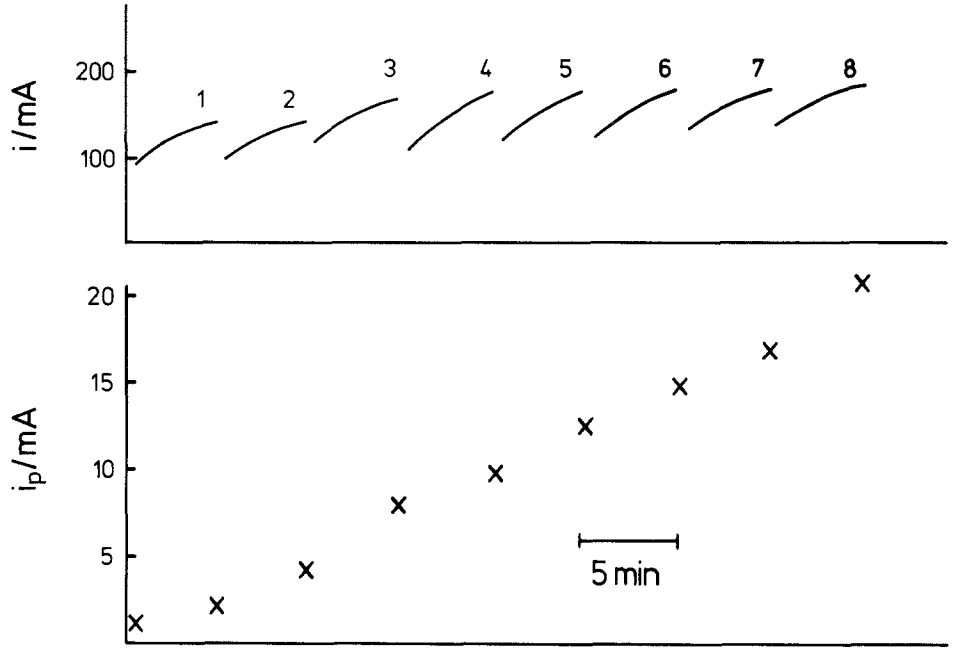

Fig. 2. Behaviour of an (initially) type I electrode in 0.5 M H_2SO_4, subjected to 8 treatments of *in situ* hydrogen evolution at -1800 mV versus SCE for 5 minutes each time. Top curves, hydrogen evolution currents; bottom points, i_p recorded on 6th cycle of DCCV response, between each hydrogen treatment.

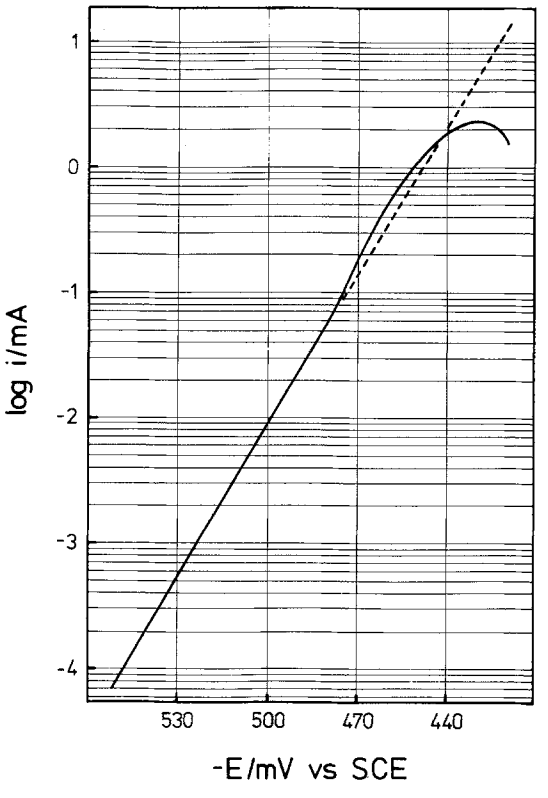

Fig. 3. Tafel plot for the $Pb^0 \rightarrow Pb^{II}$ reaction on an uncycled type II electrode, $\nu = 2\ mV\ s^{-1}$, 0.5 M H_2SO_4. Full ohmic compensation used.

3.2. *Linear potential scans, Tafel slope measurements*

Using slow linear potential scans we measured Tafel slopes for both the Pb→Pb(II) dissolution reaction and for the hydrogen evolution. The Tafel plot for the Pb→Pb(II) reaction is illustrated in Fig. 3. Using an H_2SO_4 concentration of 0.5 M ensured no complications due to overlap of the hydrogen current and the dissolution current, and it turned out that we could measure the Tafel slope for the dissolution reaction accurately over three orders of magnitude. The result was that

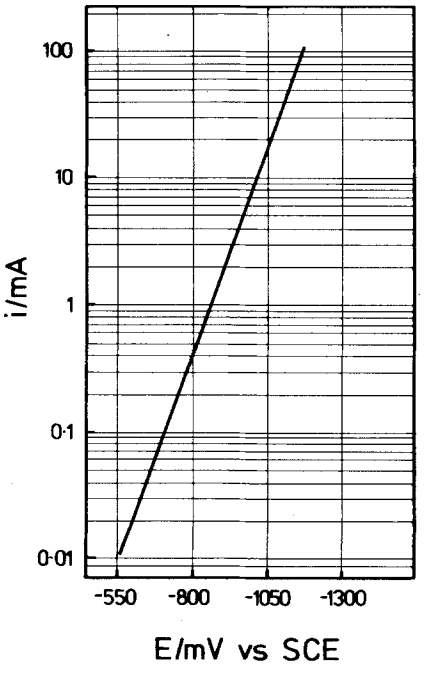

Fig. 4. Tafel plot for the hydrogen evolution reaction on a type III electrode, $\nu = 10\ mV\ s^{-1}$, 0.5 M H_2SO_4. Full ohmic compensation used.

$\partial \log i/\partial \eta$ was equal to $(25.2\ mV)^{-1}$ at 21° C. In our measurements the onset of electrocrystallization became evident at −480 mV versus SCE. The current due to the electrocrystallization process therefore distorted higher values of i in the Tafel measurement, and hence data points more positive than −480 mV were rejected. Tafel measurements were also obtained in various other electrolytes, and the results are gathered in Table 1.

A Tafel slope measurement for the hydrogen evolution reaction is shown in Fig. 4. In this case we used scan rates of $10\ mV\ s^{-1}$ to avoid accumulation of gas bubbles at the higher currents. The measured Tafel slopes were ~ 145 ± 10 mV for the three electrolytes listed in Table 1. This value differs considerably from the 'classical' value of

Table 1

Electrolyte	*Tafel slope for H_2 evolution* (mV)	*Tafel slope for Pb dissolution* (mV)
0.5 M H_2SO_4	~ 150	25.2 ± 0.5
0.5 M $(NH_4)_2SO_4$, pH 4.04	~ 140	26.8 ± 0.5
0.5 M Na_2SO_4, pH 4.02	~ 150	27.0 ± 0.5

120 mV reported in the literature [5] and we are unable at present to account for this difference. Using different cell designs (rotating discs, vertical cathodes, etc.), different electrode pretreatments, and different scan rates, we were nevertheless quite unable to record values as low as 120 mV.

3.3. *Linear potential scans, peak parameter measurements*

We also used the linear potential scan technique to investigate the variation of i_p with scan rate for the reaction $Pb \rightarrow PbSO_4$. In the first series of experiments we employed type III electrodes which were treated by evolving hydrogen for precisely five minutes between measurements. A single scan was traced each time through the $Pb/PbSO_4$ region, whereupon a further five minutes of hydrogen evolution pretreatment was begun. On alternate scans, a scan rate of 200 mV s^{-1} was always used as an internal reproducibility check. In between the 200 mV s^{-1} scans various different scan rates were employed. Data obtained in this way are shown as the upper line in Fig. 5. Each datum point corresponds to at least two measurements, but the reproducibility was such that the differences between points obtained under identical conditions were of the same order of magnitude as the thickness of the lines traced out by the fast-response pen recorder. Thus only single-datum points are plotted on the diagram. The data are plotted in the form of log i_p versus log ν in order to bring all points on to one plot. The gradient of the log–log plot was found to be 0.63 ± 0.03.

In a second series of experiments type III electrodes were cycled at 200 mV s^{-1} (producing a steady voltammogram) and as the i–$\eta(t)$ curve traversed the current zero prior to the $PbSO_4$ peak a new scan rate was switched in. This procedure led to a series of surprising results, typified here by Fig. 6. At slower scan speeds than 200 mV s^{-1} the $Pb \rightarrow PbSO_4$ peak was resolved into two distinct components separated by ~ 20 mV. The variation of i_p with scan rate for the first of the two peaks is shown as the lower line in Fig. 5. The gradient $\partial \log i_p / \partial \log \nu$ was found to be 0.62 ± 0.05, in close agreement with that obtained above. A similar value was found for the second peak but with a somewhat larger scatter of data points.

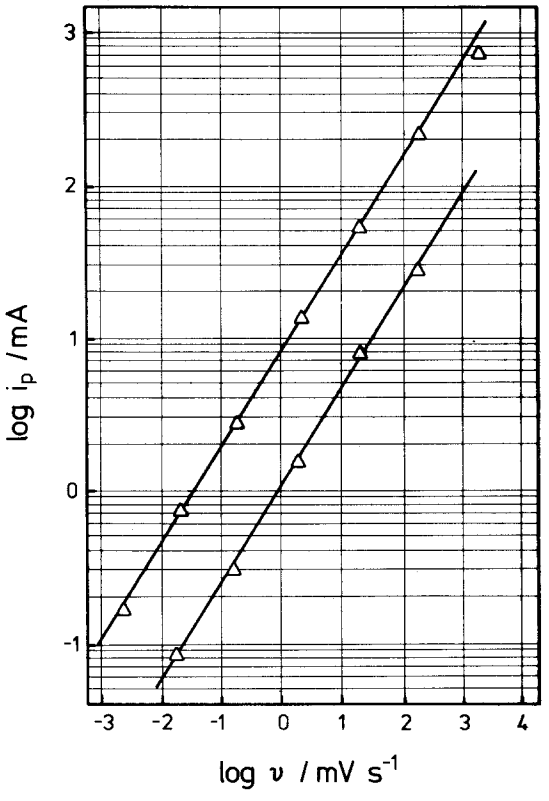

Fig. 5. Variation of i_p with scan rate (ν) in 0.5 M H_2SO_4. Upper line, hydrogen-pretreated type III electrodes, lower line, cycled, then interrupted, type III electrodes. In both cases full ohmic compensation was used.

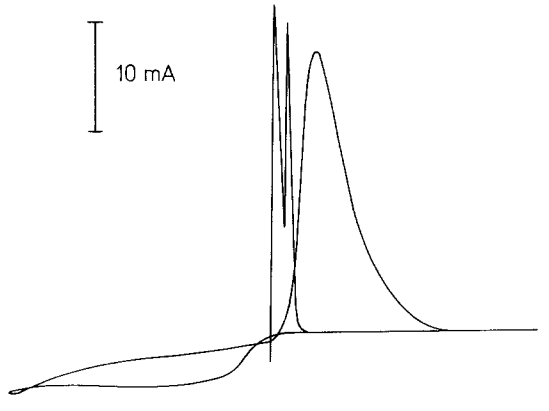

Fig. 6. Effect of switching to slow scan rate during steady cycling of a type III electrode in 0.5 M H_2SO_4. Broad single peak recorded at $\nu = 200$ mV s^{-1}. Narrow doublet recorded at 0.2 mV s^{-1}, with vertical scale amplified 100× for clarity. Scan limits were −1500 and −500 mV versus Hg_2SO_4, full ohmic compensation used.

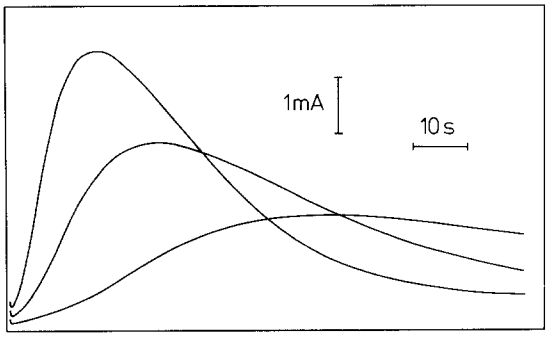

Fig. 7. Current–time transients recorded after potential steps to −920 mV (top curve), −925 mV (middle curve), and −930 mV (bottom curve); potentials versus Hg_2SO_4 in the same solution. Solution 0.5 M H_2SO_4, full ohmic compensation used.

3.4. *Potential step measurements*

Potential step measurements, like the linear potential scan measurements, were also carried out on type III electrodes, pretreated each time with hydrogen evolution. A sequence of *i–t* transients observed as a result of steps to various potentials is illustrated in Fig. 7. It was found that full ohmic compensation in these measurements was very important; for example, addition of 1 Ω uncompensated resistance resulted in approximately 50% reduction in i_p in the data reported in Fig. 7. As in the linear potential scan measurements, treating the electrode with hydrogen evolution between measurements ensured a high level of reproducibility in this data.

Using the positive-feedback, ohmic compensation facility it was possible to investigate the rising sections of the *i–t* transients at values of *i* much greater than those caused by background currents (due to H_2 evolution, etc.). In this way it was found that *i* increased proportionally to t^3 in the initial region. This dependence was seen most clearly at high potentials, i.e. $E > -900$ mV versus Hg_2SO_4. At somewhat lower potentials (−900 to −940 mV versus Hg_2SO_4) the t^3 dependence was difficult to resolve because of background currents, and because of the presence of a small falling transient at short times (just visible in Fig. 7). In the absence of full ohmic compensation all data became distorted to the extent that *i* seemingly varied somewhere between t^1 and t^2.

The *i–t* transient maximum parameters i_m and

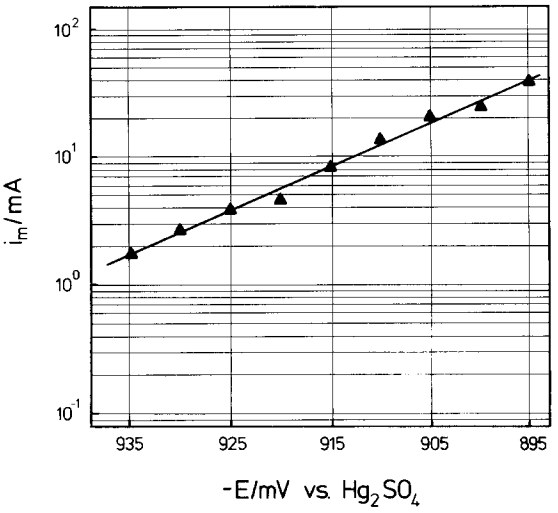

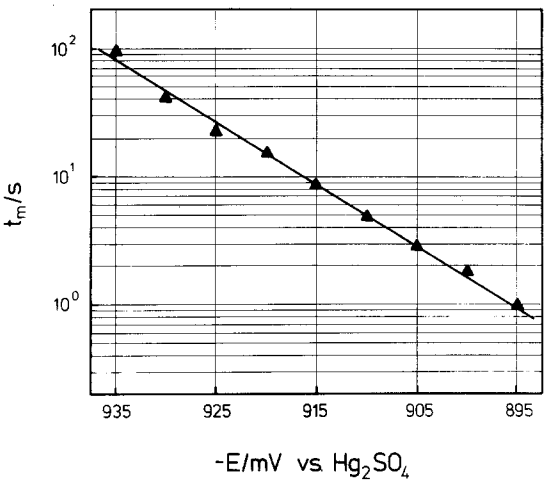

Fig. 8. (a) Current maxima in current–time transients (i_m) plotted as a function of step potential. (b) Time taken to achieve current maxima t_m plotted as a function of step potential.

t_m (obtained using full ohmic compensation) are plotted logarithmically in Figs. 8a and b. Assuming linearity of these plots, the gradients are found to be

$$\frac{\partial \log i_m}{\partial E} \simeq (31 \pm 3\,\text{mV})^{-1} \qquad (12)$$

$$-\frac{\partial \log t_m}{\partial E} \simeq (21 \pm 3\,\text{mV})^{-1} \qquad (13)$$

over the experimental range of potential from −935 mV to −895 mV versus Hg_2SO_4.

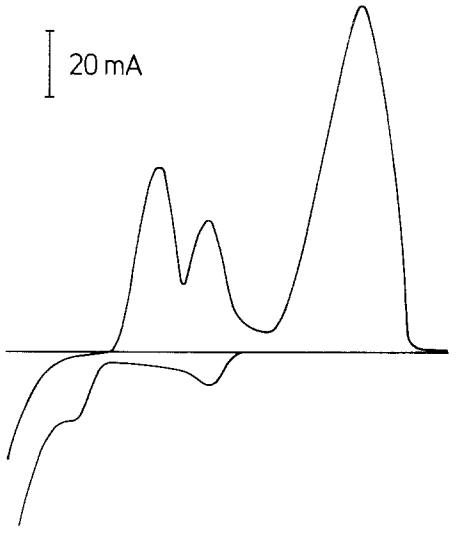

Fig. 9. Linear potential scan from −1300 mV to +100 mV versus Hg_2SO_4 on the type III electrode after 200 cycles through PbO_2 region. $\nu = 200$ mV s^{-1}, first scan with full ohmic compensation used.

3.5. *Other measurements*

We also investigated the effects of cycling lead electrodes beyond the $PbSO_4$ region, i.e. through the PbO_2 region and into oxygen evolution. Having cycled the electrodes several hundred times back and forth through the PbO_2 region at 200 mV s^{-1} they were then returned to −1800 mV versus Hg_2SO_4 for a further two hours and finally scanned through the $PbSO_4$ region. Electrodes pretreated in this way behaved very differently to type III electrodes used in the work described above. The first scans recorded after the PbO_2 pretreatment took the form shown in Fig. 9. Three peaks were apparent on the positive scan and two peaks on the reverse scan. On the second and subsequent scans the second positive-going peak disappeared and the third peak disappeared after about the 15th cycle (Fig. 10). Subsequent scans were then virtually indistinguishable from those recorded on type III electrodes. These results suggested that after type III electrodes had been cycled through the PbO_2 region and restored to negative potentials, some surface species remained intact and modified subsequent cycling behaviour in the potential range −1300 mV to +100 mV versus Hg_2SO_4. Although we were unable to identify the second positive-going peak in the

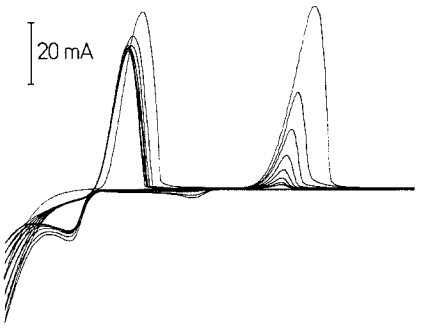

Fig. 10. As in Fig. 9, but beginning at the third successive scan and continuing to the 10th.

voltammogram we believe that the third (more persistent) positive-going peak corresponded to the formation of a PbO species [6]. It seems likely that the formation of PbO at this type of electrode occurred because of the presence of residual crystalline nuclei of PbO or PbO_2, which, though resistant to reduction, nevertheless were able to act as sites at which the PbO could be formed. Not surprisingly, using type III electrodes a voltammetric peak due to PbO formation was not observed because of the absence of appropriate seed nuclei.

4. Conclusions

We have investigated the formation of $PbSO_4$ on Pb in 0.5 M H_2SO_4 solution using electrodes principally of the type III category. With full ohmic compensation for the electrolyte component of the *iR* drop the type III electrodes exhibited excellent reproducibility, as observed in both potential step measurements and in voltammetric (continuous cycling) measurements. Our data showed that on cycled type III lead surfaces the formation of crystalline $PbSO_4$ could be resolved into *two* distinct processes using linear potential scans. In these scans, the separation between the peak potentials of the two processes was ~ 20 mV. Using uncycled type III electrodes it was not possible to observe more than one peak. The possibility therefore exists that when only one peak is seemingly observed for the formation of $PbSO_4$, by whatever technique is employed, then the single peak may possibly be composed of two separate processes which are poorly resolved. This fact necessarily makes any analysis of experimental data conditional upon how many

processes are assumed to be operating in the first place. For example, it is not clear if the single voltammetric peak recorded on uncycled type III electrodes corresponds to one well-resolved process or two poorly-resolved processes. Thus comparison of our results with the theory outlined in the introduction is necessarily restricted.

However some tests can be made. Let us consider the potential step measurements of the type shown in Fig. 7. It is reasonable to suppose that if these transients are, in reality, composed of two superimposed components then the first component dominates the leading edge of the transient (the t^3 dependence) and also that this first component contributes to the maximum to quite a high degree. The second component, on the other hand, can then be imagined to contribute in part to the maximum and to play a major role in the final tailing behaviour of the i–t curve. Therefore we shall proceed on the assumption that the rising transient and the maximum can be taken to be reasonable measures of the first process. If, of course, the transient corresponds to only one process after all, then our analysis will not be affected provided that it is understood that the data then refer to the entire transient.

Since the best-resolved transients rise as t^3, we use the model of progressive nucleation to test our data. (It can easily be shown that our model of progressive nucleation predicts a t^3 rise of current at short times.) In particular, Equation 10 allows us to investigate the potential dependence of the appearance rate of crystals (A). Within an accuracy of one or two orders of magnitude, we can also estimate the constant in Equation 10 by assuming that the constants in Equations 8 and 9 are comparable with those obtained in the theory of [3]. We obtain

$$i_m^2 t_m^3 \simeq (2 \times 10^{10}) A^{-1} \qquad (14)$$

where i_m is expressed in mA, t_m is expressed in s, and A is expressed in nuclei $cm^{-2}\ s^{-1}$. The results are shown in Fig. 11. Assuming linearity of the plot, the gradient $\partial \log A/\partial \eta$ has the value $\sim 10\,mV^{-1}$. Making the (reasonable) assumption that the appearance rate of crystals (A) varies with potential identically as J (the nucleation rate) it follows that the observed nucleation rates are $\gg 1$ nucleus $cm^{-2}\ s^{-1}$. Hence we are observing nucleation at driving forces considerably higher than

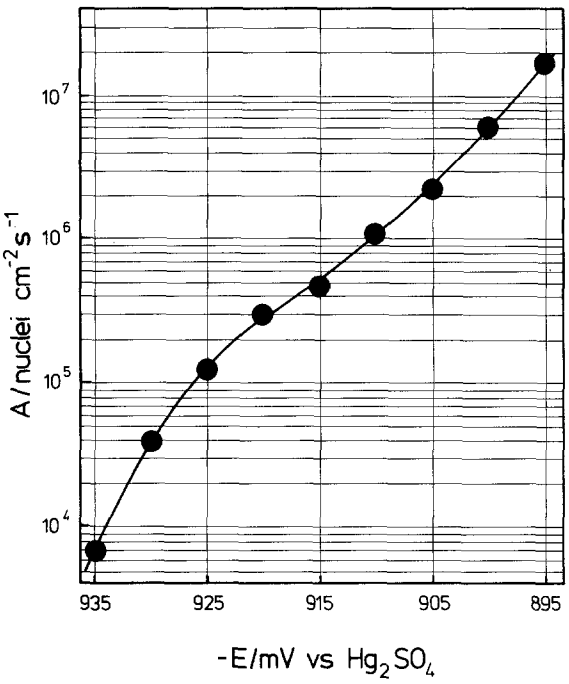

Fig. 11. Variation of the appearance rate of $PbSO_4$ crystals as a function of step potential, according to the described model.

those treated by thermodynamic theories of nucleation. This suggests that the following atomistic (kinetic) expression for J is appropriate [7]

$$J = J_0 \exp \frac{(n_c + 1 - \alpha) nF}{RT} \eta \qquad (15)$$

where J_0 contains a number of constants (defined in the original paper) and n_c is the number of 'molecules' of $PbSO_4$ characterizing the critical size of nucleus required for crystal growth. Taking $\alpha \simeq 0.5$ it follows that $n_c \simeq 1$, i.e. the nucleation is taking place on 'active sites'. That is to say, nucleation is catalyzed by defects etc. present on the lead surface. On purely physical grounds we can see that this is not unreasonable, because copious hydrogen evolution was used in the present work to activate the lead surface prior to recording experimental data.

It is important to note the differences between data recorded on hydrogen-evolution pretreated electrodes and data recorded on cycled electrodes. On cycled electrodes it was always possible to resolve two peaks for the formation of $PbSO_4$ provided sufficiently slow scan rates were employed, whereas we were unable to observe this at all on

hydrogen-treated surfaces. We suspect that one of the two peaks in the cycled-electrode case may be connected with residual $PbSO_4$ crystals which did not reduce back on previous scans, but which were removed at potentials corresponding to hydrogen evolution. However, this point has yet to be fully resolved.

Unfortunately, our mathematical model has not yet been extended to include linear potential scans so the values of $\partial \log i_p / \partial \log \nu \simeq 0.62$ cannot be fully interpreted. The experimental data prove unequivocally however that the rates of crystallization of $PbSO_4$ are not controlled by diffusion of any species through solution, since diffusion controlled reactions would be expected to give values of $\partial \log i_p / \partial \log \nu$ identically equal to 0.5, or *less*, and this is not observed. This conclusion applies to both hydrogen-pretreated type III electrodes and cycled type III electrodes.

We would like to stress that the progressive nucleation mechanism proposed by us for the hydrogen-pretreated electrodes cannot be simply extended to include cycled electrodes because of the complicating influence of residual $PbSO_4$ nulcei observed by ourselves [4] and others [8–11]. During the first 6 cycles or so there is a build-up of residual $PbSO_4$ nuclei upon cycling and this naturally leads to a change in mechanism. In particular the peak(s) observed in the voltammograms for the $Pb \rightarrow PbSO_4$ reaction shift to more negative potentials and decrease in height. This corresponds to a change from progressive nucleation towards an instantaneous nucleation mechanism [8–11]. It is interesting to note that this process results in a steady *increase* in the number of crystals (observed by scanning electron microscopy), yet corresponds to a steady *decrease* in the charge passed in forming the complete layer. This is precisely the effect predicted by Equation 5.

Equation 5 also allows us to qualitatively understand the different behaviour of type I and type III electrodes [4]. We suppose that type I electrodes have a large number of small surface defects, whereas type III electrodes additionally have a small number of very large defects (pits). Nucleation at the type III electrodes occurs preferentially at the small number of pits, leading to few nuclei and hence thicker layers of $PbSO_4$ crystals.

Another interesting observation connected with Equation 5 concerns the discriminant curve cyclic voltammetric (DCCV) response of type II electrodes reported in our previous paper [4]. Up to about the sixth cycle these electrodes showed a falling i_p as a function of cycle number, but then showed a steadily rising i_p over several hundred cycles. The initial fall in i_p was connected with the change in nucleation mechanism from 'progressive' to 'instantaneous' as described above. However, during the later steady increase in the peak current/cycle number curve a gradual 'ripening' of the $PbSO_4$ crystals was revealed by scanning electron microscopy, i.e. the total number of crystals *decreased* as i_p (and q_{Total}) *increased*. This latter observation is also in line with Equation [5]. We attribute this decrease in the crystal population to differences in solubility of $PbSO_4$ crystals as a function of their size (cf. Ostwald ripening). Thus as $PbSO_4$ crystals were reduced on each backward voltammetric scan the smaller crystals dissolved preferentially, whereas subsequent crystal growth on forward voltammetric scans occurred at already-existing larger crystals. The large crystals thus grew larger because of the comparative ease of instantaneous nucleation compared with progressive nucleation (progressive nucleation requires higher overpotentials). On the other hand, during dissolution the smaller crystals dissolved preferentially which may be understood from both thermodynamic and kinetic considerations. Thermodynamics predicts that small crystals are more soluble than large crystals (the Gibbs–Thomson equation) and from a kinetic viewpoint, diffusion zones with small radii of curvature (such as those surrounding small crystals) are more 'aggressive' than those with large radii of curvature (such as those surrounding large crystals). Thus from both points of view small crystals are expected to dissolve faster than large crystals. Thus preferred growth at large crystals and preferred dissolution at small crystals gradually resulted, upon cycling, in a diminution in the overall population of crystals. The net result after many cycles was a large amount of $PbSO_4$ formed on the forward scans ('discharge') but considerable difficulty in reducing it back on reverse scans ('charge').

Finally we note that cycling lead electrodes to very positive potentials (oxygen evolution, Fig. 9 and 10) resulted in radically different behaviour of the $Pb/PbSO_4$ reaction on subsequent scans. The

presence of an additional peak at ~ 300 mV versus Hg_2SO_4 (which is the potential at which oxides of the type $PbO \cdot PbSO_4$ etc. are expected [6]) gave rise to the suggestion that this reaction was 'catalyzed' by the presence of residual nuclei, in this case of PbO or PbO_2. The gradual disappearance of this peak upon cycling at negative potentials tended to confirm this view.

In conclusion we may summarize our results on type III electrodes as follows. Beginning with an initially $PbSO_4$-free surface, lead dissolved as Pb^{2+} ions according to the overall reaction

$$Pb \underset{}{\overset{-2e}{\rightleftharpoons}} Pb^{2+}(\text{solution})$$

for which a Tafel slope of ~ 26 mV was observed. At more positive potentials crystal growth of $PbSO_4$ (solid) began by a process of heterogeneous nucleation at active sites on the lead surface. The crystallization process continued until it was self-inhibited by spatial interactions within the layer of crystals. The rate determining step in the crystallization process could not be identified but it occurred at the peripheries of the growing crystals. Transport to growth sites in the crystal was very fast, and possibly faster than the charge-transfer process (N.B. the positive deviation of the Tafel line at the onset of crystallization in Fig. [3]). This suggested that the charge-transfer process was accelerated overall during crystal growth, either because of a surface area increase due to local Pb^{2+} dissolution or because the necessity to fully solvate Pb^{2+} was lost. This could easily have been the case if transport from the lead surface to the growth positions in the crystals occurred by rapid surface diffusion over the faces of the crystals.

The back reaction $PbSO_4 \rightarrow Pb^0$ was not identically the reverse of the forward reaction. The $PbSO_4$ crystals first needed to dissolve into solution penetrating the layer, and thence the Pb^{2+} ions diffused slowly back to the electrode surface. If insufficient time was allowed for this process before a subsequent forward scan then a build-up of residual crystals occurred. (Powerful evidence for the involvement of solution species involved in the back reaction was provided by scanning electron microscopy; lead dendrites could be observed as a result of the discharge of Pb^{2+} ions proceeding through localized diffusion zones [4].) However we stress that solution species played no rate-determining role in the kinetics of the forward crystallization reaction.

Comparison of our experimental data with the models outlined in the introduction was necessarily limited, but Equations 5, 10 and 11 provided a certain amount of physical insight into processes occurring within the layer of $PbSO_4$ crystals. The log–log plot of i_p versus ν also proved interesting, because of the dependence found for i_p on $\nu^{0.62}$. This result suggests that extension of our mathematical model to include linear potential scans may shed some light on the cycling behaviour of lead electrodes.

Acknowledgements

One of us (S.F.) would like to thank the Department of Transport of the Government of South Australia for a fellowship.

References

(A more extensive compilation may be found in Part 1.)

[1] S. Fletcher and D. Matthews, *J. Appl. Electrochem.* 11 (1981) 1.
[2] *Idem, ibid* 11 (1981) 7.
[3] R. D. Armstrong, M. Fleischmann and H. R. Thirsk, *J. Electroanal. Chem.* 11 (1966) 208.
[4] S. Fletcher and D. Matthews, *J. Appl. Electrochem.* 11 (1981) 11.
[5] J. O'M Bockris and S. Srinivasan, *Electrochim. Acta* 9 (1964) 31.
[6] D. Pavlov and R. Popova, *ibid* 15 (1970) 1483.
[7] A. Milchev, S. Stoyanov and R. Kaischev, *Thin Solid Films* 22 (1974) 255.
[8] G. Archdale and J. A. Harrison, *J. Electroanal. Chem.* 34 (1972) 21.
[9] *Idem, ibid* 39 (1972) 357.
[10] *Idem, ibid* 43 (1973) 321.
[11] *Idem, ibid* 47 (1973) 93.